Originally published as:

RESEARCH ARTICLE

Key Points:
- Improved skills of snowmelt simulation using a daily active temperature method
- Uncertainties in projected flows and underlying causes are analyzed
- Future changes in extreme flows are addressed using a probabilistic approach

Supporting Information:
- Readme
- Figure S1
- Figure S2
- Figure S3
- Table S1
- Text S1

Correspondence to:
X. Wang,
xywang86@126.com

Climate change and probabilistic scenario of streamflow extremes in an alpine region

Tao Yang[1,2], Xiaoyan Wang[2], Zhongbo Yu[2], Valentina Krysanova[3], Xi Chen[1], Franklin W. Schwartz[4], and Edward A. Sudicky[5]

[1]State Key Laboratory of Desert and Oasis Ecology, Xinjiang Institute of Ecology and Geography, Chinese Academy of Sciences, Urumqi, China, [2]State Key Laboratory of Hydrology-Water Resources and Hydraulic Engineering, Center for Global Change and Water Cycle, Hohai University, Nanjing, China, [3]Research Domain II: Climate Impacts and Vulnerabilities, Potsdam Institute for Climate Impact Research, Telegrafenberg, Potsdam, Germany, [4]School of Earth Sciences, 275 Mendenhall Laboratory, Ohio State University, Columbus, Ohio, USA, [5]Department of Earth and Environmental Sciences, University of Waterloo, Waterloo, Ontario, Canada

Abstract Future projections of streamflow extremes are of paramount significance in assessing the climate impacts on social and natural systems, particularly for the Himalayan alpine region in the Tibetan Plateau known as the Asian water tower. This study strives to quantify the uncertainties from different sources in simulating future extreme flows and seeks to construct reliable scenarios of future extreme flows for the headwater catchment of the Yellow River Basin in the 21st century. The results can be formulated as follows: (1) The revised snow model based on a daily active temperature method is superior to the commonly used degree-day method in simulating snowmelt processes. (2) In general, hydrological models contribute more uncertainties than the downscaling methods in high flow and low flow over the cryospheric alpine regions characterized by the snow-rainfall-induced runoff processes under most scenarios. Meanwhile, impacts to uncertainty vary with time. (3) The ultimate probability of high flow exhibits a downward trend in future by using an unconditional method, whereas positive changes in the probability of low flow are projected. The method in the work includes a variety of influence from different contributing factors (e.g., downscaling models, hydrological models, model parameters, and their simulation skills) on streamflow projection, therefore can offer more information (i.e., different percentiles of flow and uncertainty ranges) for future water resource planning compared with the purely deterministic approaches. Hence, the results are beneficial to boost our current methodologies of climate impact research in the Himalayan alpine zone.

1. Introduction

The increasing concentration of greenhouse gases since preindustrial time has led to global warming and changes in precipitation pattern and other climate variables, which is likely to lead to a more vigorous hydrological cycle. These changes in turn affect the runoff regimes of rivers and may change water availability [*Middelkoop et al.*, 2001]. In particular, extreme events such as floods, debris flows, and droughts are likely to increase in frequency, duration, and magnitude in climate sensitive regions [*Yang et al.*, 2010; *Yang et al.*, 2012]. Therefore, public interest and awareness of importance of the extreme climatic and hydrological events have increased sharply in recent years. To address these issues, the impact study of climate change on hydrological extremes in the upcoming century has become a hot spot, both for hydrological science research, water and watershed management, and adaptation and development strategies [*Piao et al.*, 2010].

The Yellow River in North China is currently under immense pressure from various competitive users influenced by social, political, and legislative conditions. Due to a significant contribution of runoff, the headwater catchment of the Yellow River is known as "the cistern of the Yellow River" [*Xu et al.*, 2009]. It is located in a high-elevation and cold area, where hydrological and ecological processes are highly sensitive to climate change. Therefore, growing amount of studies on climate impact in this region have been found in recent years. For instance, *Lan et al.* [2010] found that the runoff processes in the headwater region of the Yellow River are more sensitive to precipitation change than to temperature change. *Hu et al.* [2011] showed by means of correlation analysis between climatic variables and streamflow that the decrease in streamflow in 1959–2008 resulted from decreasing precipitation in wet season together with increasing temperature.

In the past, a variety of hydrological models have been widely used in climate impact studies to formulate future water resource management and development strategies. For instance, *Xu et al.* [2009] applied four global circulation models (GCMs), two downscaling methods, and Soil and Water Assessment Tool (SWAT) model in the region. Results indicate that mean streamflow will decrease in the future. A distributed hydrological model for the Yellow River Basin has been developed by incorporating the remote sensing technique and used to simulate the natural runoff without a consideration of water abstraction [*Cong et al.*, 2009]. *Immerzeel et al.* [2010] studied climate change impact on the Asian water towers (i.e., Indus, Ganges, Brahmaputra, Yangtze, and Yellow Rivers) using a revised snowmelt runoff model and climate scenarios from five GCMs. Similar studies have been conducted [e.g., *Milly et al.*, 2005; *Taye et al.*, 2010] to assess climate impact on streamflow extremes in the last decade. Yet most of the aforementioned studies only considered limited uncertainty sources (e.g., GCMs or hydrological models) in assessing the potential impacts of climate change on regional water resources or extreme flow. This surely introduces considerable uncertainties into the projection results, consequently leading to a high decision risk in water resources and ecoenvironment management. Thus, a comprehensive approach allowing to evaluate influences of various uncertainties is needed in climate impact studies.

Wilby and Harris [2006] developed a probabilistic framework for assessing uncertainties in climate change impacts in projecting low-flow scenarios for the River Thames, UK. The framework incorporated four GCMs, two greenhouse gas emission scenarios, two statistical downscaling techniques, two hydrologic models, and different sets of hydrologic model parameters. With a consideration of a number of uncertainties in streamflow projection, this approach provides a potentially beneficial means to quantify uncertainties in climate impact studies. However, runoff processes in the Himalayan alpine regions generally differ from those in the humid zones [*Wilby and Harris*, 2006]: runoff recharge source is jointly composed of precipitation, snowmelt, and glacial melt. Thus, streamflow extremes in the cryospheric alpine regions are strongly affected by precipitation and temperature and therefore are more sensitive to climate change than in the humid regions. As an important hydrological process in alpine regions, snowmelt is generally simulated by means of the degree-day method based on the daily mean temperature worldwide [*Ji and Kang*, 2013]. Actually, temperature often varies from positive one to negative one within 1 day, and the accumulated hourly positive temperature (i.e., the daily active temperature) has a more profound influence on the snowmelt. Thereafter, current modeling approach of streamflow extremes under the context of climate change in the zones has an urgent need to boost.

Therefore, this study strives to identify the uncertainty sources in projecting extreme flows and to address the potential impact of climate change on streamflow extremes in the headwater catchment of Yellow River by using the probabilistic framework. Toward this end, the article aims (1) to construct and testify skills of a variety of statistical downscaling models and hydrological models in reproducing daily temperature, evaporation, precipitation, snowmelt, streamflow, and streamflow extremes; (2) to quantify the uncertainty from different impact factors in modeling future extreme flows using a conditional analysis method; and (3) to build two sets of probabilistic scenarios of high flows and low flows incorporating a range of downscaling methods, hydrological models, parameter sets, and emission scenarios using an unconditional approach. The study results can offer valuable insights into the modeling framework of extreme river flows in support of water disaster mitigation, ecoenvironmental restoration, and management in the Himalayan alpine regions in Asia and other similar regions worldwide.

2. Study Area and Data Set

2.1. Study Area

The source region of the Yellow River refers to the catchment above the Longyang Gorge between 96°~101°30′E and 33°45′~37°05′N, with a contributing area of 121,000 km^2 upstream of Tangnaihai station (Figure 1). It belongs to the Great Himalayan region [*Yellow River Conservancy Commission*, 2002]. Providing an approximately 38% of the total water discharge of the Yellow River, it is called "water tower of the Yellow River and North China." The mean altitude of this area is about 4000 m. It is surrounded by high mountains with an altitude over 5000 m. The region is dominated by a semihumid monsoon climate. The annual average precipitation is about 450 mm. More than 70% of the total annual precipitation falls in the high-flow season from July to October. The annual average air temperature varies between −4°C and 2°C from southeast to northwest [*Xu et al.*, 2009].
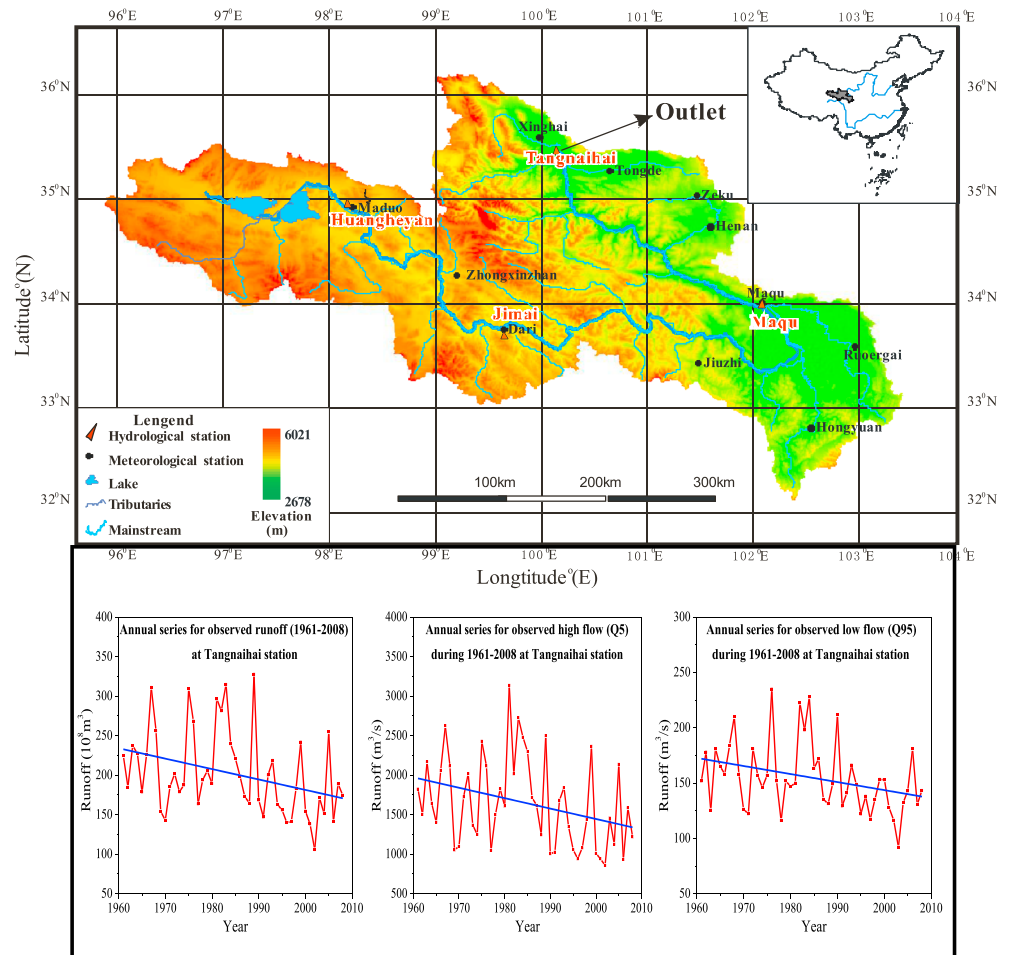
Figure 1. Map of the alpine headwater catchment of the Yellow River Basin in Himalayas and trends in the annual mean and extreme streamflows during 1961–2008 at the Tangnaihai station.

The glacier and frozen areas at the high altitudes are very sensitive to climate variation and change [*Yang et al.*, 2013a, 2013b]. Even slight changes of climate could lead to changes in hydrological processes in the region, hence impacting the water availability in the Yellow River and North China. Different from most large rivers across the world, the Yellow River is confronting a flow-decreasing period, particularly in the past decade [*Piao et al.*, 2010; *Yang et al.*, 2008]. Decreasing trends in annual mean and extreme streamflow have been identified since 1990s in the source region of the Yellow River (see Figure 1). Therefore, a critical question arises: How could this water, limited, large, and important river, sustain the future increased socioeconomic development in North China? Is the ceased flow happened in the lower Yellow River during 1990s possible to reoccur in the future? The work seeks to construct more reliable scenarios of streamflow projection to answer some of the critical questions by using the probabilistic approach.

2.2. Data

The observed daily precipitation, temperature, wind speed, relative humidity and sunshine duration, and pan evaporation data (1961–2005) at 11 meteorological stations (Table 1) and streamflow data for three hydrological stations (Jimai, Maqu, and Tangnaihai) in the region were collected from the National Climate Center, China Meteorological Administration, and the Hydrology Bureau, the Yellow River Conservancy Commission, and used in this study. A digital elevation model GTOPO30 (1 km) was employed. The vegetation data with the resolution of 1 km were derived from the global land cover facility (GLCF) data.

Twenty-six different atmospheric variables were obtained from (1) the interpolated daily reanalysis data set of National Centers for Environmental Prediction (NCEP)/National Center for Atmospheric Research for

Table 1. List of 11 Meteorological Gauges (1961–2005) in the Headwater Region of the Yellow River (Source of Data: The National Center of Climate, China)

Site Name	Site Number	Longitude	Latitude	Average Annual Temperature (°C)	Average Annual Precipitation (mm)
Xinghai	52943	99.98°E	35.58°N	1.36	353.6
Tongde	52957	100.65°E	35.27°N	0.38	429.7
Zeke	52968	101.47°E	35.03°N	−2.12	474.3
Maduo	56033	98.22°E	34.92°N	−3.72	308.2
Zhongxin zhan	56041	99.20°E	34.27°N	−3.79	459.3
Dari	56046	99.65°E	33.75°N	−0.88	543.3
Henan	56065	101.60°E	34.73°N	0.31	580.4
Jiuzhi	56067	101.48°E	33.43°N	0.61	762.2
Maqu	56074	102.08°E	34.00°N	1.53	602.3
Ruoergai	56079	102.97°E	33.58°N	1.11	647.6
Hongyuan	56173	102.55°E	32.80°N	1.43	753.0

1961–2000 at a spatial scale of 3.75° (longitude) × 2.5° (latitude) and (2) outputs of scenarios A2 and B2 of Hadley Centre coupled model version 3 (HadCM3) from 1961 to 2099, both with a spatial resolution of 3.75° (longitude) × 2.5° (latitude). The HadCM3 outputs were chosen due to relatively better performance in modeling temperature and precipitation in the East Asian regions [*Jiang et al.*, 2005]. Meanwhile, *Thomas and Kim* [2008] estimated the robustness of climate models from three different Climate Model Intercomparison Projects (CMIPs), suggesting that HadCM3 is better in simulating current climate than other models. Subsequently, a quantile-quantile mapping transformation [*Boe et al.*, 2007; *Themeßl et al.*, 2011] was used to correct GCM outputs. The steps are the following: for a given variable, a correction function depending on the quantile was first generated, by means of matching the cumulative density function (CDF) of simulations in baseline period with the CDF of the reanalysis data. Then, the correction function was applied to adjust the value of given variable under climate scenario quantile by quantile [*Boe et al.*, 2007].

3. Methodology

3.1. Downscaling Methods

3.1.1. The Statistical Downscaling Method

The statistical downscaling method (SDSM) used in our study is a hybrid of a stochastic weather generator and regression methods [*Wilby et al.*, 2003]. This method includes a built-in transform function for the sake of obtaining secondary data series of the predictand and/or the predictor that have stronger correlations than the original data series. *Diaz-Nieto and Wilby* [2005] demonstrated that the SDSM model has several advantages over conventional "change factor" methods, where new temporal sequences of (extreme) events can be generated for future climate scenario assessment. The SDSM is recommended as an effective tool for climate impact studies in many regions worldwide [e.g., *Kim et al.*, 2006]. Application of HadCM3 outputs in conjunction with SDSM was widely done in the Chinese studies during the past years [e.g., *Xu et al.*, 2009; *Chu et al.*, 2010].

As a preliminary basis for this study, statistical downscaling of extremes of temperature and precipitation in the headwater catchment of the Yellow River has been conducted based on the HadCM3 and SDSM [*Wang et al.*, 2012]. Results indicated that the model skills for temperature extremes are perfect, and for precipitation extremes are acceptable. The details described by *Wang et al.* [2012] are not addressed in this article.

3.1.2. The Artificial Neural Network Downscaling Model

The artificial neural network downscaling models (ANNs) refer to the multilayer perceptions used to establish relationships between the input variables and the dependent output variables. The models are characterized by nonlinear nature, which makes the ANNs more efficient in identifying and representing relationships using noisy data [*Hewitson and Crane*, 1996]. The back-propagation [*Wasserman*, 1989] neural network model applied in this study is the most commonly used ANN model. In past years, this neural network model has been widely used in downscaling precipitation, where the highly nonlinear processes are involved that cannot be captured well by other methods [e.g., *Coulibaly et al.*, 2005; *Schoof and Pryor*, 2001].

In this case, ANN model is trained to be able to represent the relationship between large-scale atmospheric variables (predictor) and local scale observed variables (predictand, e.g., precipitation and temperature).

The steps to construct an ANN model are the following: first, potential predictor variables (NCEP reanalysis data) are screened, as has been shown in the paper of *Wang et al.* [2012]. Then the ANN models with variable number of hidden nodes are trained using selected predictor variables as input, and thereby, the best performing network with the higher Nash–Sutcliffe efficiency and lower percent bias (or bias) is selected. Finally, the ANN model with the best performing network is driven by predictors from climate model(s) for producing downscaled scenarios of future climate change.

3.2. Hydrological Models

Hydrological models provide valuable means for quantitative simulation and prediction of catchment runoff processes that are required for efficient management of water resource systems. After an improvement of snow accumulation and melt component based on a daily active temperature method, the Xinanjiang (XAJ) model [*Zhao et al.*, 1980], TOPMODEL [*Beven and Kirby*, 1979], and HBV model [*Bergström*, 1995] were collectively applied in the runoff simulation in the study area. The description of the three models as well as the revised snowmelt module can be found in the supporting information.

The reason why the three conceptual hydrological models are used in this work is supported by following points: (1) The source region of the Yellow River is characterized by a lack of in situ observations. Hence, the validation of hydrological models is confronted with a large uncertainty, especially for the more complex process-based hydrological models (e.g., Soil and Water Assessment Tool (SWAT) and Variable Infiltration Capacity (VIC) model), which require extensive data sets (e.g., gridded climatic data, topography, and soil and vegetation data) and have complicated schemes of parameter estimation. Besides, uncertainty estimation for the complex process-based hydrological models is computationally intensive. This explains why such models were not included. (2) In recent years, there were some studies and reports [e.g., *Xu et al.*, 2009; *Chen et al.*, 2013] on hydrological modeling in the source region of the Yellow River. They collectively suggested that simple conceptual models [*Chen et al.*, 2013] can work better than the process-based semidistributed models (e.g., SWAT [*Xu et al.*, 2009]) under the circumstance of limited data availability. (3) In this work, a probabilistic approach for climate impact study is used, and a large number of simulations are involved in this method. Many unresolved issues on how to properly estimate parameter uncertainty of semidistributed and distributed models still exist, making it difficult to use distributed models in our study.

In the past, these three hydrological models have been widely used in climate change impact assessment worldwide [e.g., *Camero et al.*, 2000; *Jiang et al.*, 2007; *Driessen et al.*, 2010]. Meanwhile, in view of restrictions on the application of complex semidistributed models, the three models were hereby employed in the work.

3.3. Measures of Model Performance

The hydrological model efficiency is assessed by percent bias (PBIAS) [*Gupta et al.*, 1999], Nash–Sutcliffe efficiency (NSE) [*Nash and Sutcliffe*, 1970], and Nash–Sutcliffe efficiency with logarithmic values (lnNSE). The NSE is defined as

$$\mathrm{NSE} = 1 - \frac{\sum_{i=1}^{n} (O_i - S_i)^2}{\sum_{i=1}^{n} (O_i - \overline{O})^2} \tag{1}$$

with

$$\overline{O} = \frac{1}{n} \sum_{i=1}^{n} O_i \tag{2}$$

where n is the number of time steps, O_i is the observed discharge at time step i, and S_i is the simulated discharge at time step i.

NSE is found to be not very sensitive to the performance in modeling low flow [*Gupta et al.*, 2009; *Krause et al.*, 2005]. To offset the restriction, lnNSE, giving more weight to the low-flow values [*Shafii and Smedt*, 2009; *Krause et al.*, 2005], is applied

$$\ln \mathrm{NSE} = 1 - \frac{\sum_{i=1}^{n} (\ln O_i - \ln S_i)^2}{\sum_{i=1}^{n} (\ln O_i - \ln \overline{O})^2} \tag{3}$$
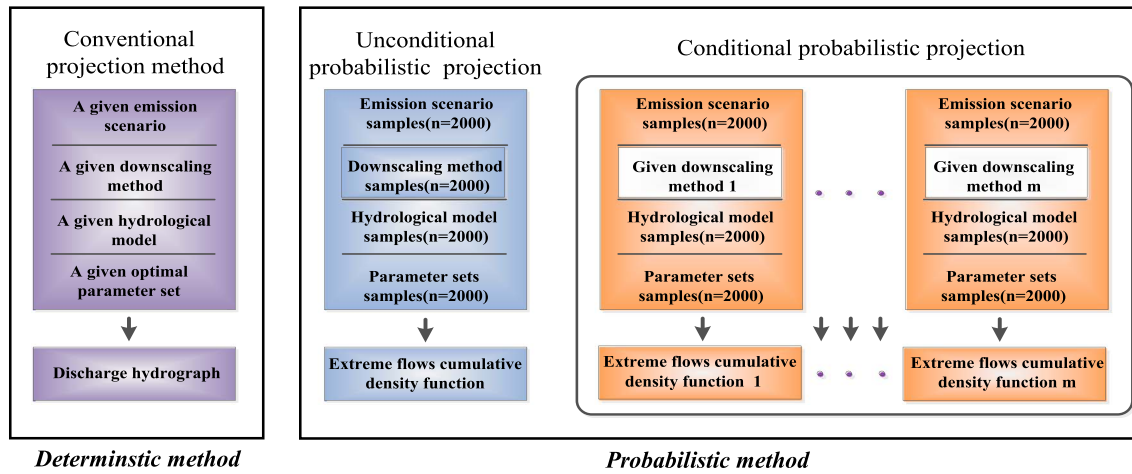
Figure 2. The schematic view of the conventional projection method and two probabilistic projection methods (unconditional and conditional) for climate impact studies.

The average tendency of the simulated data to be larger or smaller than their observed counterparts is measured by PBIAS or BIAS. They are defined as

$$\text{PBIAS} = \left[\frac{\sum_{i=1}^{n}(O_i - S_i) \times 100}{\sum_{i=1}^{n} O_i} \right] \tag{4}$$

$$\text{BIAS} = \frac{1}{n}\sum_{i=1}^{n}(O_i - S_i) \tag{5}$$

The dispersion degree of variables (RS) [*Hundecha and Bardossy*, 2008] is applied to estimate the performance of the downscaling model:

$$\text{RS} = \frac{S_{\text{sim}}}{S_{\text{obs}}} \tag{6}$$

where S_{sim} and S_{obs} are the standard deviations of the modeled and observed indices, respectively.

3.4. The Framework of Probabilistic Streamflow Projection

The framework consists of unconditional and conditional probabilistic projecting method. The former can be used to construct probabilistic and more reliable runoff scenarios from a range of emission scenarios, downscaling methods, hydrological models, and their parameter sets, while the latter can be applied to quantify uncertainties due to each component in the modeling climate change impact on runoff. The general schematic view is shown in Figure 2, where the probabilistic approaches are compared with the conventional method and where uncertainty induced by downscaling method is taken as an example to illustrate the conditional approach. In the unconditional method, emission scenarios, downscaling methods, hydrological models, and parameter sets are involved in the Monte Carlo analysis. It is performed many times until finally the cumulative density functions (CDFs) for high flow and low flow (Q5 and Q95) are obtained.

In a single task of the conditional method, for example, in case of the downscaling method, each downscaling method is constant, while emission scenarios, hydrological models, and parameters are varying within a valid range. Consequently, the corresponding cumulative density functions (CDFs) are estimated. To obtain stationary results, a test to identify the impacts of different sample size on CDF was committed by means of probabilistic projections based on 2000, 4000, and 6000 runs.

3.4.1. Construction of Unconditional Probabilistic Scenarios

In order to generate a set of probabilistic results from a range of emission scenarios, downscaling methods, hydrological models, and model parameter sets, probabilistic projections in the annual high flow (Q5)
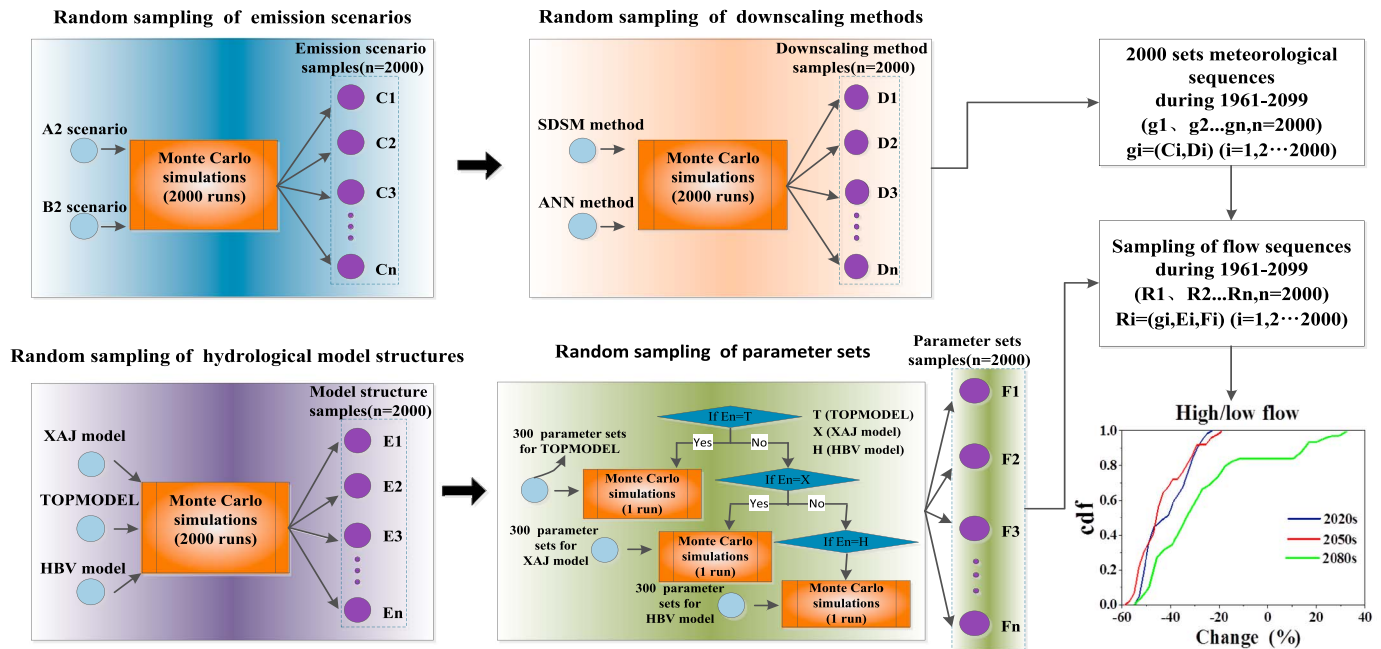
Figure 3. The approach of unconditional probabilistic projection of extreme flows using the three hydrological models, 300 parameter sets in each of them, two downscaling methods, and two emission scenarios. Note that the ith meteorological inputs (g_i) are used to generate the ith flow sequence (R_i) for 1961–2099, in conjunction with the chosen hydrological model (E_i) and parameter set (F_i).

and low flow (Q95) are constructed. Figure 3 shows the approach of creating probabilistic projections of change in high and low flow with 2000 runs. Three steps are done to obtain future probabilistic scenarios.

(1) An emission scenario (C1, C2…C2000), compatible with HadCM3 climate projection (including A2 and B2 emission scenarios), and a downscaling method (D1, D2…D2000 from SDSM or ANN downscaling method) with a consideration of its NSEs and PBIAS (or BIAS) are randomly selected using Monte Carlo simulation. Next, the downscaling method (D_i) in conjunction with emission scenario (C_i) is used to generate the long-term (1961–2099) meteorological (i.e., temperature, evaporation, and precipitation) time series (g_i, $i = 1…2000$) according to the equation "$g_i = (C_i, D_i)$." It should be noted that in total, only four different meteorological time series (combining two emission scenarios with two downscaling methods) are created and then used for 2000 runs ($g_1, g_2…g_{2000}$). (2) A random choice of one of three hydrological models ($E_1, E_2,…E_{2000}$) and the corresponding parameter set ($F_1, F_2,…F_{2000}$) is done. In this step, the parameter sets are from 300 skillful simulations in the reference period. (3) Two-thousand annual series of extreme high and low flow are estimated according to the equation "$R_i = (g_i, E_i, F_i)$." *Each series* represents the ith meteorological inputs (g_i) used to generate the ith flow sequence (R_i) for 1961–2099, in conjunction with the chosen hydrological model (E_i) and parameter set (F_i). Finally, the mean annual Q5 and Q95 are calculated in three time periods (2020s: 2010–2039, 2050s: 2040–2069, and 2080s: 2070–2099) and compared with the baseline (1961–1990) to evaluate hydrological changes. The changes are presented by cumulative density functions (CDFs).

Similar with *Wilby and Harris* [2006], the A2 and B2 emission scenarios are assigned with equal weights (0.5) in this work. Weighting downscaling methods is slightly complex than hydrological models. Because temperatures both have positive and negative values, downscaling methods are therefore weighted by NSE and BIAS when simulating temperature. Whereas, NSE and PBIAS are used in simulating daily precipitation and evaporation. In this work, the weights are 0.48 for SDSM and 0.52 for ANN. The parameter sets of the 300 most skillful simulations in the reference period, selected from a total of 10,000 parameter sets generated by the Monte Carlo simulation, are employed. The hydrological models and parameter sets are weighted by NSE and PBIAS in high flow, while lnNSE and PBIAS are used in low flow. The below part presents how different hydrological models are weighted in high-flow projection. Low-flow projection also follows the similar procedure.

The initial weights (M_x, M_T, and M_H) for the three hydrological models are from their NSEs (a_1 for XAJ model, a_2 for TOPMODEL, and a_3 for HBV) in simulating high flow during 1961–2005:

$$M_x = \frac{a_1}{a_1 + a_2 + a_3}; \quad M_T = \frac{a_2}{a_1 + a_2 + a_3}; \quad M_H = \frac{a_3}{a_1 + a_2 + a_3}$$

where M_x, M_T, and M_H represent the weights assigned to the XAJ, TOPMODEL, and HBV models. The subsequent weights to the three hydrological models (N_x, N_T, and N_H) are estimated according to the absolute value of PBIAS in simulating high flow during 1961–2005. Hence, the final weights (W_x, W_T, and W_H) used in this study are

$$W_X = \frac{M_X + N_X}{2}; \quad W_T = \frac{M_T + N_T}{2}; \quad W_H = \frac{M_H + N_H}{2} \; (W_x + W_T + W_H = 1)$$

In high-flow (Q5) projection, the weights are 0.35 (HBV), 0.33 (XAJ), and 0.32 (TOPMODEL), while 0.33 (HBV), 0.37(XAJ), and 0.30 (TOPMODEL) are used as weights in low-flow projection (Q95). The model weights work in Monte Carlo simulations (2000, 4000, and 6000 runs) to estimate final CDFs. In the step, a random number D ($0 \le D \le 1$) is generated to determine which hydrological model is involved in a single simulation. If $D < W_x$, XAJ model will participate in the first simulation. If D lies in [W_x, $W_x + W_T$], TOPMODEL will be involved. Otherwise, HBV will be included.

3.4.2. Construction of Conditional Probabilistic Scenarios

To quantitatively assess uncertainties from different sources, the conditional probabilistic projections in Q5 and Q95 were constructed on the basis of Monte Carlo simulations. Figure S1 in the supporting information shows the approach of constructing cumulative density functions of conditional extreme flows. After a SDSM downscaling method is chosen as a constant component in a simulation task (Figure S1a in the supporting information), the following steps are as same as in the unconditional method. In a single assessment, SDSM downscaling method is constant, while emission scenarios, hydrological models, and parameters are varying within a valid range until finally the cumulative density function (CDF) of extreme flows is obtained. By this means, a series of CDFs of future flows depending on the SDSM, ANN, XAJ model, TOPMODEL, and HBV (Figures S1b–S1e in the supporting information) can be generated and compared. Therefore, the uncertainty induced by different impact factors (downscaling methods and hydrological models) can be quantitatively assessed. Note that the steps to obtain future probabilistic scenarios from 2000, 4000, and 6000 runs are similar. The difference only lies in the number of Monte Carlo simulations.

4. Results and Discussions

4.1. Calibration and Validation of Downscaling Models and Hydrological Models

4.1.1. Validation of the Artificial Neural Network Downscaling Model ANN

The SDSM-based downscaling in the study region has been reported in our previous work [*Wang et al.*, 2012]. In this section, we show the performance of the ANN model in reproducing the mean and extreme climate parameters. The Nash–Sutcliffe efficiency (NSE) measure, PBIAS (or BIAS), and the degree of dispersion (RS) were used as criteria for the performance assessment. Table 2 is a summary of the performance skills of the ANN downscaling method for the indices [*Wang et al.*, 2012] of mean temperature, evaporation, and precipitation in the calibration (1961–1990) and validation (1991–2000) periods. It is evident that the method performed better in reproducing the temperature-related indices (NSE ≥ 0.95). The performance in reproducing precipitation and evaporation-related indices (NSE ≥ 0.63, PBIAS < 10.0%) is acceptable. Meanwhile, the standard deviation differences (RS) between the observation and the simulation (Table 2) suggest that the model can reproduce the temporal variability of the temperature indices well (RS ≥ 0.95). However, the variability of evaporation and precipitation indices is slightly lower (0.92 ≥ RS ≥ 0.75). A comparison of the observed and simulated daily mean temperature, precipitation, and evaporation during 1961–2000 are shown in Figure S2 in the supporting information. It can be seen that the daily mean temperature (T_{mean}) is reproduced well, with a slight underestimation from February to July. In comparison, the model capability in simulating daily precipitation (P) and evaporation (E) varies seasonally. The simulated precipitation matched well with the observations in all seasons except summer. Regarding evaporation, an underestimation in summer and an overestimation in winter are found.

Table 2. Performance Assessment for the Artificial Neural Network Downscaling Model in the Calibration (1961–1990) and Validation (1991–2000) Periods

	Calibration			Validation		
Predictands	NSE	BIAS/PBIAS	RS	NSE	BIAS/PBIAS	RS
T_{mean}	0.96	−0.01°C	1.00	0.95	0.00°C	0.97
T_{max}	0.96	0.33°C	0.98	0.96	0.47°C	0.97
T_{min}	0.96	−0.63°C	0.98	0.95	−0.73°C	0.95
E	0.68	0.1%	0.81	0.65	0.7%	0.82
E_{max}	0.74	7.9%	0.82	0.65	8.6%	0.75
P	0.70	2.4%	0.83	0.65	1.2%	0.85
P_{max}	0.80	6.7%	0.81	0.63	9.8%	0.79
Px5d	0.92	2.7%	0.92	0.88	5.7%	0.91

4.1.2. Intercomparison of Two Snowmelt Approaches for Simulating Snow Depth

Snowmelt simulations using two approaches during 1995 to 2006 are conducted and compared. Table S1 in the supporting information shows a summary of percent bias (PBIAS) for two snowmelt methods (1995–2006). To investigate the spatiotemporal snowmelt change over a data sparse large basin, the remote sensing technique is used to estimate snowmelt and compare with simulations for ungauged areas. *Che et al.* [2008] estimated snow depth derived from passive microwave satellite remote sensing data (scanning multichannel microwave radiometer (SMMR) from 1978 to 1987 and Special Sensor Microwave/Imager (SSM/I) from 1987 to 2006) in China. The algorithm considered the influences from vegetation, wet snow, precipitation, cold desert, and frozen ground. Furthermore, the algorithm is dynamically adjusted based on the seasonal variation of grain size and snow density. This result exhibits good potential in snow depth estimation and has been widely used in snow studies over China [e.g., *Ji and Kang*, 2013]. In this work, three typical regions in the study domain (Figure S3 in the supporting information) with different land cover are
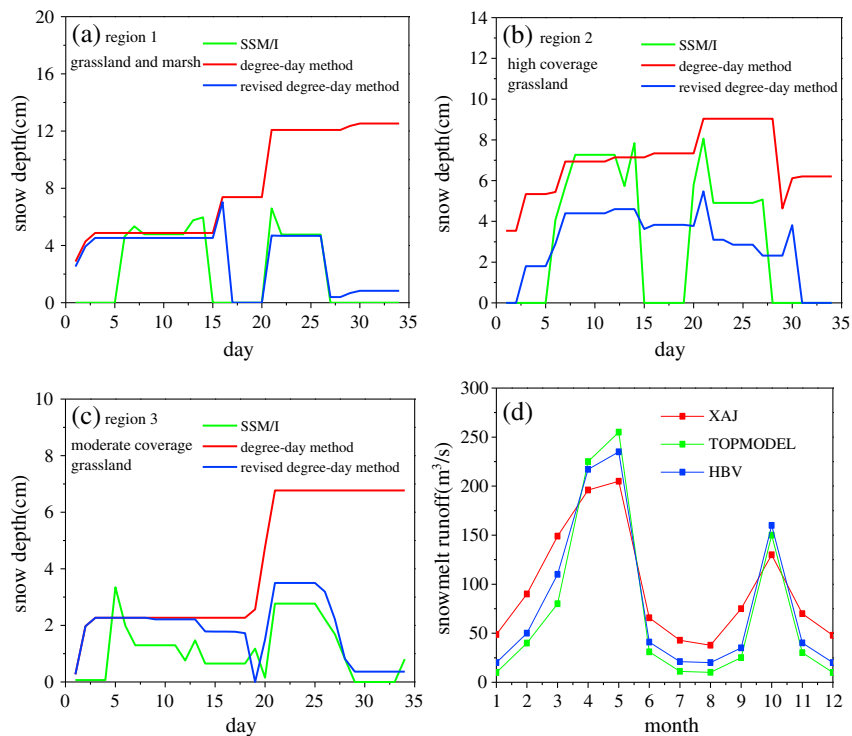

Figure 4. Comparison of the SSM/I and simulated (using two methods) daily snow depth during 1 February 2004 to 5 March 2004 in the three typical subregions with (a–c) different land cover and (d) seasonal pattern of simulated monthly average snowmelt runoff for the whole basin by hydrological models.

Table 3. Skill Scores of the Three Hydrological Models in the Calibration (1961–1990) and Validation (1991–2005) Periods

Gauges	Periods	Measures of Skill	XAJ	TOPMODEL	HBV
Tangnaihai	Calibration 1961–1990	lnNSE	0.84	0.72	0.77
		PBIAS (%)	2.01	1.25	2.70
		NSE	0.81	0.78	0.83
	Validation 1991–2005	lnNSE	0.82	0.63	0.75
		PBIAS (%)	3.35	−3.44	2.41
		NSE	0.79	0.70	0.81
Maqu	Calibration 1961–1990	lnNSE	0.81	0.54	0.76
		PBIAS (%)	2.16	−7.16	5.20
		NSE	0.81	0.67	0.80
	Validation 1991–2005	lnNSE	0.73	0.48	0.74
		PBIAS (%)	−15.85	−12.24	−4.60
		NSE	0.68	0.61	0.78
Jimai	Calibration 1961–1990	lnNSE	0.52	0.47	0.53
		PBIAS (%)	8.09	−9.70	4.97
		NSE	0.64	0.51	0.76
	Validation 1991–2005	lnNSE	0.46	0.42	0.51
		PBIAS (%)	12.26	−13.40	−7.61
		NSE	0.51	0.49	0.61

used to compare changes of the daily snow depth derived from Special Sensor Microwave/Imager (SSM/I) [*Che et al.*, 2008] and simulated by two methods during 1 February 2004 to 5 March 2004 (Figures 4a–4c). In general, the revised model is better in capturing the daily snow depth dynamics. Particularly, it is capable of simulating 0 cm snow depth. For instance, region 1 was characterized by negative daily mean temperature from February to early March in 2004. Therefore, snowmelt based on the general degree-day method would not occur, leading to a continuous increase of the simulated snow depth (Figure 4a). However, hourly positive temperature occurred in some days. This enables an accurate snowmelt simulation by the revised snowmelt model. Therefore, the revised snowmelt model based on the daily active temperature is integrated into hydrological models for simulation.

4.1.3. Performance of the Three Hydrological Models in Reproducing Historical Streamflow

This section presents an intercomparison of performances of the three hydrological models in reproducing observed daily streamflow and extremes in the period 1961–2005. The historical records of the three hydrological stations over the period of 1961–2005 were split into two periods: 1961–1990 for calibration and 1991–2005 for validation. Table 3 is a summary of Nash–Sutcliffe efficiency (NSE), percent bias (PBIAS), and logarithmic Nash–Sutcliffe efficiency (lnNSE) for the three hydrological models at three gauges in the headwater catchment of the Yellow River. In general, acceptable results are obtained for most stations in both the calibration and validation periods. Especially, the good results are achieved for the Tangnaihai station (outlet), with NSE higher than 0.70, lnNSE higher than 0.60, and PBIAS lower than 4% for all the three models. This suggests that all the three models can commonly generate satisfactory simulations in the basin. In addition, the seasonal pattern of snowmelt runoff simulated by the three hydrological models is consistent during 1961–2005, characterized by two peaks in May and October (Figure 4d). However, the difference between the models in reproducing monthly snowmelt runoff is found in winter and spring. Unfortunately, no in situ information is available on observed snowmelt depth and density in this basin, forming a challenge to evaluate the skills of hydrological models in snowmelt runoff simulation.

Compared to the good performance of the daily streamflow simulation at the Tangnaihai station, simulations for the high flow (Q5) at this station are slightly poorer during 1961–2005, and the low-flow (Q95) simulations are even worse. Nevertheless, the trends of extreme flow series are modeled quite well. Figures 5a–5c show the trends of the observed and simulated annual Q5 during 1961–2005. The downward trend is found in the observed Q5 series. The descending trend is also well detected by all the three hydrological models. Furthermore, the P values estimated by the Mann–Kendall test indicate the trends significance at the 0.1 level ($P < 0.1$). Meanwhile, the downward trend of low flow shown by the observed Q95 series (Figures 5d–5f) is well reproduced by the three hydrological models. The significance of trends at the 0.1 level is achieved by two models.
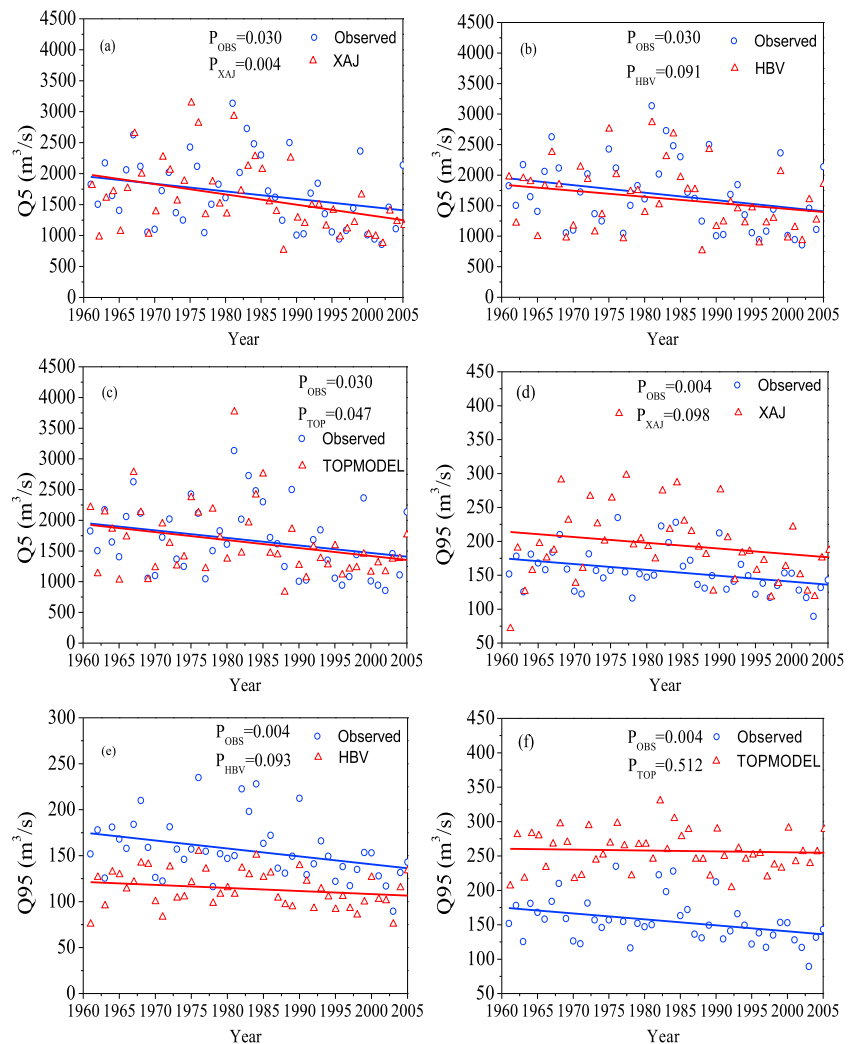
Figure 5. The observed and simulated high flows (Q5) by (a) XAJ, (b) HBV, and (c) TOPMODEL and low flows (Q95) by (d) XAJ, (e) HBV, and (f) TOPMODEL at the Tangnaihai station. The linear fitting curves indicate the trends and the corresponding P values detecting the significance of the trends.

4.2. Probabilistic Analysis of Climate Change Impact on Extreme Flows
4.2.1. Effects of Uncertainty Sources on Extreme Flows

The effects of uncertainty sources (statistical downscaling methods and hydrological models) on modeling extreme streamflows during three future periods are assessed using a conditional probabilistic projection approach. The results for high flow and low flow based on 2000, 4000, and 6000 runs are shown below.

4.2.1.1. High Flow

Figures 6a–6c demonstrate different percentiles (90%, 75%, 50%, 25%, and 10%) of CDFs for changes in high flows (Q5) during three future periods based on 2000 runs. The ranges of uncertainty from different sources estimated as the differences between the medians of separate conditional runs are summarized in Table 4. It can be seen that the uncertainty due to the choice of downscaling method is increasing with time. The median change in high flow in 2020s corresponding to downscaling methods is −38.7% (ANN: Figure 6a) and −42.0% (SDSM: Figure 6a). It indicates that the uncertainty range induced by the downscaling methods is minor (42.0% − 38.7% = 3.3%). In 2080s, the medians are −22.5% (ANN: Figure 6c) and −39.5% (SDSM; Figure 6c). Hereby, uncertainty induced by downscaling methods increases to 17.0%.

The uncertainty in high-flow projections triggered by hydrological models is less time dependent (Table 4). Moreover, the hydrological models reveal slightly higher uncertainties in 2020s and 2050s compared to
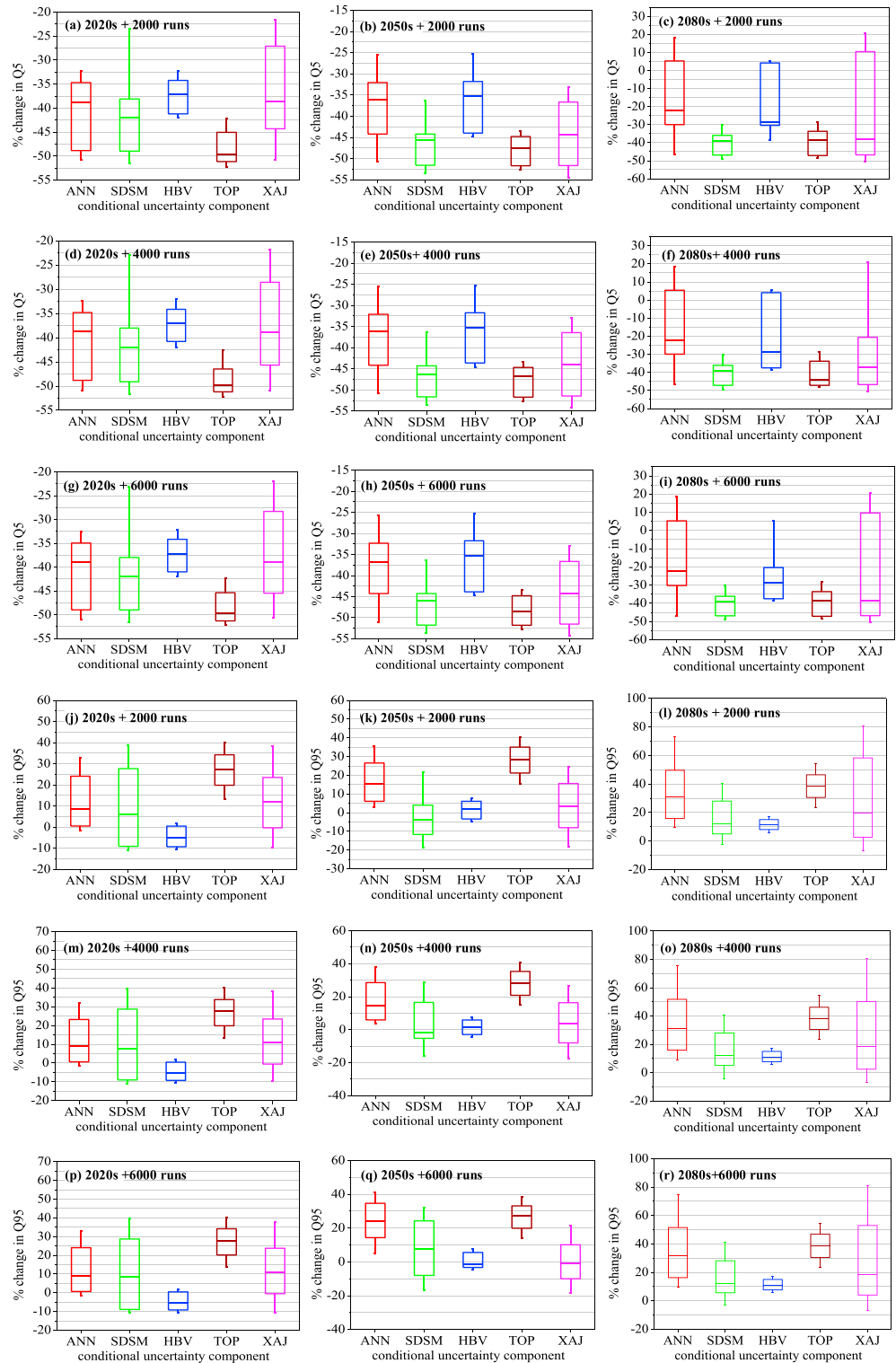
Figure 6. (a–r) Selected percentiles (90%, 75%, 50%, 25%, and 10%) of CDFs for changes in high flows (Q5) and low flows (Q95) using a conditional probabilistic projections approach with different sample sizes (2000, 4000, and 6000 runs) for three periods: 2020s, 2050s, and 2080s.

Table 4. Ranges of Uncertainty From the Downscaling Methods and Hydrological Models in the Projection of High Flow and Low Flow Based on 2000 Runs

Periods	High Flow (Q5)		Low Flow (Q95)	
	Downscaling Method	Hydrological Model	Downscaling Method	Hydrological Model
2020s	3.3%	12.2%	2.7%	32.5%
2050s	9.3%	12.5%	17.9%	26.0%
2080s	17.0%	12.0%	17.6%	28.1%

that from the downscaling methods. For instance, the median of CDFs for changes in high flow ranges from -37.3% (HBV) to -49.5% (TOPMODEL) in 2020s (Figure 6a). Hence, uncertainty introduced by hydrological models is 12.2% in 2020s and higher than 3.3% (corresponding to downscaling methods). However, the downscaling methods present a slightly higher uncertainty during 2080s in comparison with hydrological models (Figure 6c).

Therefore, it suggests the general influence of uncertainty components on high flow in the headwater catchment of the Yellow River: hydrological model > downscaling method. Similar results can be shown for CDFs of Q5 changes based on the conditional probabilistic projection (Figures 6d–6i; 4000 and 6000 runs), indicating that the influence of different sample sizes ($\geq$2000) on the high-flow projections in the headwater catchment of the Yellow River is slight.

4.2.1.2. Low Flow

The projections of the three hydrological models are distinct (Figures 6j–6r), and they contribute more significantly to uncertainty in modeling future low flows based on different sample size (2000, 4000, and 6000). In 2080s, the medians for changes in low flow range from 10.5% (HBV) to 38.6% (TOPMODEL), which is much higher than that from the downscaling methods: 30.1% (ANN) and 12.5% (SDSM) (Figure 6l). Smaller range related to the downscaling methods suggests that they contribute less to the overall uncertainty compared to the hydrological models.

It is however different compared to the results presented by *Wilby and Harris* [2006] for the Thames Basin. In their study, the hydrological models were less important contributors to the uncertainty in the modeling of low flows than the statistical downscaling methods. This could be explained as follows: The prevailing climate in the Thames Basin is mild sea climate characterized by warm and wet weather condition, and low flow occurring in summer is commonly generated by low rainfall. Whereas, the runoff processes in the source region of the Yellow River in the Tibetan Plateau are dominated by snowmelt and rainfall together. As shown in Figure 4d, the differences between the models in reproducing monthly snowmelt runoff are found in winter and spring. This indicates that low flow formed jointly by snowmelt and rainfall is more difficult to simulate, in the context of serious lack of in situ observations (both snow and rainfall) in the Tibetan alpine regions.

Besides, the hydrological models used in both studies were different. To further analyze the underlying causes leading to differences in low-flow simulation in our study by various hydrological models, the structures of hydrological models were analyzed. In TOPMODEL, the vertical water movement from the unsaturated zone to the saturated zone is estimated by a very simple linear relationship. Moreover, the assessment of the evaporation loss in the root storage zone is also very simple. These simplifications demonstrate that the runoff generation processes receive more attention, compared to the water budget accounting [*Xiong and Guo*, 2004]; hence, a moderate or even poor performance in simulating low flows is probable for TOPMODEL. In the case of HBV model, a triangular weighting function is used to describe the runoff concentration process, and uncertainties could be introduced by this simplification to a certain degree.

The methods used for snow process modeling include temperature index method (e.g., degree-day method or its variations) and energy balance approach. *Singh and Singh* [2001] pointed out that which method would be chosen depends on the type of application. The temperature index method is widely used as a practical method in the daily streamflow forecasting, with a consideration of limitations in the availability of basin observed data. This is linked with the fact that energy balance approach needs higher-input data requirements. The temperature index method has been widely used in previous studies published in world leading journals (e.g., [*Immerzeel et al.*, 2010, 2013] in Science and Nature Geoscience) focusing on streamflow
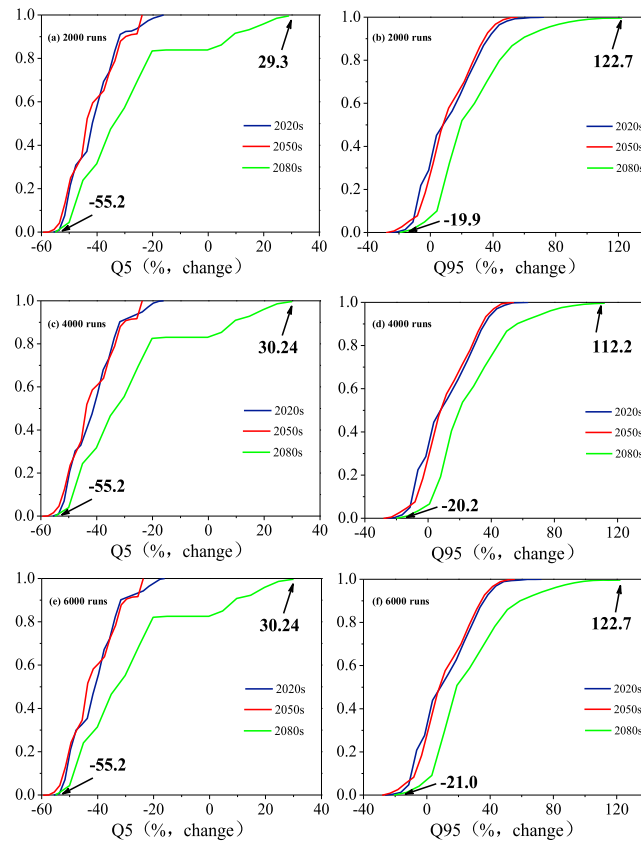
Figure 7. CDFs of changes in high flows (Q5) and low flows (Q95) using an unconditional probabilistic projections approach with different sample sizes ((a and b) 2000, (c and d) 4000, and (e and f) 6000 runs) during 2020s, 2050s, and 2080s.

simulation over the Tibetan Plateau. Thus, it is acceptable to simulate snowmelt based on the daily active temperature method in this work.

Meanwhile, permafrost is an important process for the land surface hydrology of cold regions. However, studies focusing on the simulation of the plateau's permafrost process at the regional scale are seriously limited. Frozen soil process in large-scale basins over Tibetan Plateau is characterized by complexity caused by varied topographic characteristics and serious data scarcity of in situ observations (e.g., soil moisture and soil temperature at different depths). More important, different from glacier and snow study, various state-of-the-art satellite techniques could not be used to monitor permafrost distribution and melting processes (because it is underground). Therefore, permafrost study in a large basin does not have essential data support; this forms a big challenge. These collectively restricted the evaluation and application of frozen soil parameterization scheme. This is why the frozen soil module in most hydrological models was often ignored for basin simulations over Tibetan

Plateau in the past [e.g., *Immerzeel et al.*, 2010, 2013]. However, the general impact of permafrost melt on streamflow is smaller than that of the glacier, snow, and precipitation in alpine regions, according to recent report [*Immerzeel et al.*, 2010, 2013]. Hence, the permafrost modeling has not been included into the work.

In summary, we can conclude that the hydrological models exert more important influences than the downscaling methods in the region, where runoff is generated by snowmelt and rainfall, due to the serious limit in snow and rainfall observations, applied spatial discretization scheme, and possible deficiencies in modeling snow process and frozen soil process in mountainous terrain. The data-sparsity problem is a big challenge for hydrological modeling in the Tibetan alpine regions. This is different from the findings in the Thames Basin dominated by rainfall-induced runoff processes [*Wilby and Harris*, 2006].

4.2.2. Probabilistic Projection of Extreme Flows Under Climate Change

In order to construct a set of probabilistic scenarios for extreme flows from a range of emission scenarios, statistical downscaling models, hydrological models, and parameter sets, the approach of unconditional probabilistic projection (Figure 3) was used. The results from 2000, 4000, and 6000 runs are presented in Figures 7a–7f, which suggest considerable changes in high flow: a distinct decrease in 2020s and 2050s and less certain changes (e.g., from −55.2% to 29.3% based on 2000 runs, from −55.2% to 30.24% based on 4000 runs, and from −55.2% to 30.24% based on 6000 runs; Figures 7a, 7c, and 7e) in 2080s. Still, the decrease in high flow has 82.6%–84.3% probability in the third scenario period (Figures 7a, 7c, and 7e). Those collectively indicate a general and quite certain decrease of high flows in all three future periods. Regarding the low-flow projections, they are less certain (e.g., from −19.9% to 122.7% based on 2000 runs; Figure 7b) in 2080s. Still, the probability of increase in low flow ranges from 65.1% to 68.4% (2020s), from 71.2% to 73.3% (2050s), and from 92.4% to 94.5% (2080s) based on 2000, 4000, and 6000 runs (Figures 7b, 7d, and 7f). This might help to alleviate the serious situation of water shortage for the Yellow River.

In the past, a number of studies have projected hydrological regime change in response to the climate change in the Tibetan Plateau. For example, *Xu et al.* [2009] used the SWAT model driven by climate from four GCMs (HadCM3, the Canadian Global Coupled Model CGCM2, the Centre for Climate System Research (CCSR) and CSIRO developed by Commonwealth Scientific and Industrial Research Organisation in Australia) downscaled by two downscaling methods (delta and statistical methods) to project change in the monthly streamflow in the headwater catchment of the Yellow River, suggesting a reduction of mean streamflow in the future. In our study, further steps have been implemented to address future changes in high and low flows and to evaluate uncertainties from different sources using the probabilistic approach. The method encompasses a variety of impacts from important contributing factors (e.g., downscaling models, hydrological models, parameters, and their simulation skills) on streamflow projection and thus has obvious advantages over the general deterministic method before [*Li et al.*, 2008; *Xu et al.*, 2009]. Meanwhile, the study provides more valuable information on runoff regimes (different percentiles of flow and CDFs) and uncertainty impacts. It is an important step forward on climate impact study in the Tibetan alpine regions.

5. Conclusions

General findings and results of impacts of climate change on water resources over the Tibetan Plateau using a wide range of GCMs, statistical downscaling methods, and hydrological models were presented recently by *Li et al.* [2008] and *Xu et al.* [2009]. Their results indicate that streamflow in the region is likely to decrease, which would intensify the water shortage situation in the Yellow River and North China in the 21st century. However, reports aiming to address the future changes in extreme flows (high and low flows) over the Himalayan alpine regions by means of a probabilistic framework have not been found so far. In contrast to the previous publications using the general deterministic approach, this study strives to assess the uncertainties from different sources in simulating future extreme flows and seeks to construct probabilistic and more reliable scenarios of extreme streamflows in the headwater catchment of the Yellow River Basin in the Tibetan Plateau during the 21st century. It was done by means of applying a variety of hydrological models and two statistical downscaling methods (SDSM and ANN) driven by the HadCM3 GCM model, under a range of emission scenarios. The major points can be summarized as follows:

1. The revised snowmelt module based on the daily active temperature is superior to the general degree-day method in simulating daily snow depth. It suggests that the daily active temperature is more suitable to model snowmelt processes than the daily mean temperature.
2. The uncertainties due to the downscaling methods are increasing with time in simulations of future high flow. In the study basin, the hydrological models were more important contributors to the overall uncertainty of high-flow projections in 2020s and 2050s, in comparison with the downscaling methods. However, the downscaling methods reveal a higher uncertainty in 2080s. This shows that contributors to uncertainty related to future high flow may vary with time.
3. By analyzing the uncertainty behavior for the projected low flows, it is also demonstrated that the hydrological models contribute more uncertainties than the downscaling methods in streamflow simulation over the alpine regions characterized by the snow-rainfall induced runoff processes. This is mainly from the challenge in modeling streamflow jointly formed by snowmelt and rainfall under a circumstance restricted by the limited meteohydrological ground observation. It is a major highlight of this work, which is different from the findings for the Thames Basin by *Wilby and Harris* [2006].
4. The work generates two sets of overall probabilistic projections of high and low flows with a consideration of a range of hydrological models, downscaling methods, and emission scenarios, as a comprehensive reference for the water hazard mitigation. Based on the probabilistic projections, the probabilities of positive changes in low flow are 65.1%–68.4%, 71.2%–73.3%, and 92.4%–94.5%, based on a range of Monte Carlo runs in 2020s, 2050s, and 2080s, respectively. Meanwhile, the probability of negative changes in high flow exceeds 80% for all the three periods in future.

The work addresses future changes in extreme flows using a range of downscaling methods, hydrological models, parameter sets, and emission scenarios by a probabilistic approach. The applied method can offer more and valuable information (i.e., CDFs, different percentiles of flow, and uncertainty ranges) for water resource planning compared to the purely deterministic approaches. Although some preliminary results on changes in hydrological extremes over the plateau are obtained in the present work, a lot of uncertainties

still exist in projecting extreme flows in this region. For example, the effects of uncertainty due to dynamical downscaling methods were not considered. More research works in the future, particularly using the ensemble projections by latest CMIP5-GCMs, dynamical downscaling models, and spatially distributed or semidistributed hydrological models adjusted for high-elevation and cold regions, are needed for a more profound understanding of the potential future changes in hydrological extremes in this unique area.

References

Bergström, S. (1995), The HBV model, in *Computer Models of Watershed Hydrology*, edited by V. P. Singh, pp. 443–476, Water Resources Publications, Highlands Ranch, CO.

Beven, K. J., and M. J. Kirby (1979), A physically based variable contributing area model of basin hydrology, *Hydrolog. Sci. Bull.*, *24*, 43–69.

Boe, J., L. Terray, and F. Habets (2007), Statistical and dynamical downscaling of the Seine basin climate for hydro-meteorological studies, *Int. J. Climatol.*, *27*, 1643–1655.

Camero, D., K. Beven, and P. Naden (2000), Flood frequency estimation by continuous simulation under climate change (with uncertainty), *Hydrol. Earth Syst. Sci.*, *4*(3), 393–405.

Che, T., X. Li, and R. L. Armstrong (2008), Snow depth derived from passive microwave remote-sensing data in China, *Ann. Glaciol.*, *49*, 145–154.

Chen, X., T. Yang, and X. Y. Wang (2013), Uncertainty intercomparison of different hydrological models in simulating extreme flows, *Water Resour. Manag.*, *27*(5), 1393–1409.

Chu, J., J. Xia, and C. Y. Xu (2010), Statistical downscaling of daily mean temperature, pan evaporation and precipitation for climate change scenarios in Haihe River, China, *Theor. Appl. Climatol.*, *99*(1–2), 149–161.

Cong, Z. T., D. W. Yang, and B. Gao (2009), Hydrological trend analysis in the Yellow River basin using a distributed hydrological model, *Water Resour. Res.*, *45*, W00A13, doi:10.1029/2008WR006852.

Coulibaly, P., Y. B. Dibike, and F. Anctil (2005), Downscaling precipitation and temperature with temporal neural networks, *J. Hydrometeorol.*, *6*, 483–496.

Diaz-Nieto, J., and R. L. Wilby (2005), A comparison of statistical downscaling and climate change factor methods: Impacts on low flows in the River Thames, United Kingdom, *Clim. Change*, *69*, 245–268.

Driessen, T. L. A., R. T. W. L. Hurkmans, and W. Terink (2010), The hydrological response of the Ourthe catchment to climate change as modelled by the HBV model, *Hydrol. Earth Syst. Sci.*, *14*(4), 651–665.

Gupta, H. V., S. Sorooshian, and P. O. Yapo (1999), Status of automatic calibration for hydrologic models: Comparison with multilevel expert calibration, *J. Hydrol. Eng.*, *4*, 135–143.

Gupta, H. V., H. King, K. K. Yilmaz, and G. F. Martinez (2009), Decomposition of the mean squared error and NSE performance criteria: Implications for improving hydrological modelling, *J. Hydrol.*, *377*(1–2), 80–91.

Hewitson, B. C., and R. G. Crane (1996), Climate downscaling: techniques and application, *Clim. Res.*, *7*, 85–95.

Hu, Y. R., S. Maskey, and S. Uhlenbrook (2011), Streamflow trends and climate linkages in the source region of the Yellow River, China, *Hydrol. Process.*, doi:10.1002/hyp.8069.

Hundecha, Y., and A. Bardossy (2008), Statistical downscaling of extremes of daily precipitation and temperature and construction of their future scenarios, *Int. J. Climatol.*, *28*(5), 589–610.

Immerzeel, W. W., L.-P. H. Van Beek, and M.-F. P. Bierkens (2010), Climate change will affect the Asian water towers, *Science*, *328*, 1382–1385.

Immerzeel, W. W., F. Pellicciotti, and M. F. P. Bierkens (2013), Rising river flows throughout the twenty-first century in two Himalayan glacierized watersheds, *Nat. Geosci.*, *6*, 742–745.

Ji, Z., and S. Kang (2013), Projection of snow cover changes over China under RCP scenarios, *Clim. Dyn.*, *41*, 589–600.

Jiang, D. P., H. J. Wang, and X. M. Lang (2005), Evaluation of East Asian climatology as simulated by seven coupled models, *Adv. Atmos. Sci.*, *22*(4), 479–495.

Jiang, T., Y. D. Chen, and C. Y. Xu (2007), Comparison of hydrological impacts of climate change simulated by six hydrological models in the Dongjiang Basin, South China, *J. Hydrol.*, *336*(3–4), 316–333.

Kim, S. B., H. S. Kim, and B. H. Seoh (2006), Impact of climate change on water resources in Yongdam Dam Basin, Korea, *Stoch. Environ. Res. Risk Assess.*, *21*(4), 355–373.

Krause, P., D. P. Boyle, and F. Base (2005), Comparison of different efficiency criteria for hydrological model assessment, *Adv. Geosci.*, *5*, 89–97.

Lan, Y. C., G. H. Zhao, and Y. N. Zhang (2010), Response of runoff in the source region of the Yellow River to climate warming, *Quaternary Int.*, *226*(1–2), 60–65.

Li, L., Z. C. Hao, and J. H. Wang (2008), Impact of future climate change on runoff in the head region of the Yellow River, *J. Hydrol. Eng.*, *13*(5), 347–354.

Middelkoop, H., K. Daamen, D. Gellens, W. Grabs, J. C. J. Kwadijk, H. Lang, B. W. A. H. Parmet, B. Schädler, J. Schulla, and K. Wilke (2001), Impact of climate change on hydrological regimes and water resources management in the Rhine basin, *Clim. Change*, *49*, 105–128.

Milly, P. C. D., K. A. Dunne, and A. V. Vecchia (2005), Global pattern of trends in streamflow and water availability in a changing climate, *Nature*, *415*, 514–517.

Nash, J. E., and J. V. Sutcliffe (1970), River flow forecasting through conceptual models part 1-A discussion of principles, *J. Hydrol.*, *10*(3), 282–290.

Piao, S., et al. (2010), The impacts of climate change on water resources and agriculture in China, *Nature*, *467*, 43–51.

Schoof, J., and S. C. Pryor (2001), Downscaling temperature and precipitation: a comparison of regression-based methods and artificial neural networks, *Int. J. Climatol.*, *21*, 773–790.

Shafii, M., and F. D. Smedt (2009), Multi-objective calibration of a distributed hydrological model (WetSpa) using a genetic algorithm, *Hydrol. Earth Syst. Sci.*, *13*, 2137–2149.

Singh, P., and V. P. Singh (2001), *Snow and Glacier Hydrology*, Kluwer Acad., Dordrecht, Netherlands.

Taye, M. T., V. Ntegeka, N. P. Ogiramoi, and P. Willems (2010), Assessment of climate change impact on hydrological extremes in two source regions of the Nile River Basin, *Hydrol. Earth Syst. Sci.*, *15*, 209–222, doi:10.5194/hess-15-209-2011.

Themeßl, M. J., A. Gobiet, and A. Leuprecht (2011), Empirical-statistical downscaling and error correction of daily precipitation from regional climate models, *Int. J. Climatol.*, *31*, 1530–1544.

Thomas, R., and J. Kim (2008), How well do coupled models simulate today's climate?, *Bull. Am. Meteorol. Soc.*, *89*, 303–311.

Wang, X., T. Yang, and Q. Shao (2012), Statistical downscaling of extremes of precipitation and temperature and construction of their future scenarios in an elevated and cold zone, *Stoch. Environ. Res. Risk Assess.*, *26*, 405–418.

Wasserman, P. (1989), *Neural Computing: Theory and Practice*, Van Nostrand Reynold, New York.

Wilby, R. L., and I. Harris (2006), A framework for assessing uncertainties in climate change impacts: Low-flow scenarios for the River Thames, UK, *Water Resour. Res.*, *42*, W02419, doi:10.1029/2005WR004065.

Wilby, R. L., O. J. Tomlinson, and C. W. Dawson (2003), Multi-site simulation of precipitation by conditional resampling, *Clim. Res.*, *23*, 183–194.

Xiong, L. H., and S. L. Guo (2004), Effects of the catchment runoff coefficient on the performance of TOPMODEL in rainfall-runoff modeling, *Hydrol. Process.*, *18*, 1823–1836.

Xu, Z., F. Zhao, and J. Li (2009), Response of streamflow to climate change in the headwater catchment of the Yellow River basin, *Quaternary Int.*, *208*, 62–75.

Yang, T., Q. Zhang, Y. D. Chen, X. Tao, C.-Y. Xu, and X. Chen (2008), A spatial assessment of hydrologic alteration caused by dam construction in the middle and lower Yellow River, China, *Hydrol. Process.*, *22*, 3829–3843.

Yang, T., Q. Shao, Z. Hao, X. Chen, Z. Zhang, C. Y. Xu, and L. Sun (2010), Regional frequency analysis and spatio-temporal pattern characterization of rainfall extremes in Pearl River Basin, Southern China, *J. Hydrol.*, *380*(3–4), 386–405.

Yang, T., X. B. Hao, Q. X. Shao, C.-Y. Xu, C. Y. Zhao, X. Chen, and W. G. Wang (2012), Multi-model ensemble projections in temperature and precipitation extremes of the Tibetan Plateau in the 21st century, *Global Planet. Change*, *80–81*, 1–13.

Yang, T., et al. (2013a), Review of advances in hydrologic science in China in the last decades: Impact study of climate change and human activities, *J. Hydrol. Eng.*, *18*(11), 1380–1384.

Yang, T., C. Wang, Z. Yu, and F. Xu (2013b), Characterization of spatio-temporal patterns for various GRACE-and GLDAS-born estimates for changes of global terrestrial water storage, *Global Planet. Change*, *109*, 30–37.

Yellow River Conservancy Commission (2002), Yellow River Basin Planning [in Chinese], YRCC website. [Available at http://www.yrcc.gov.cn/.]

Zhao, R. J., Y. Zhuang, and L. Fang (1980), The Xinanjiang model, Hydrological Forecasting Proceedings Oxford Symposium, 129, pp. 351–356, IAHS publication.